John von Neumann Institute for Computing



Structural and Electronic Properties of Clean and Adsorbate-Covered (001) Surfaces of Cubic SiC

Xiangyang Peng, Jürgen Wieferink, Peter Krüger, and Johannes Pollmann

published in

NIC Symposium 2006 ,
G. Münster, D. Wolf, M. Kremer (Editors),
John von Neumann Institute for Computing, Jülich,
NIC Series, Vol. **32**, ISBN 3-00-017351-X, pp. 135-142, 2006.

© 2006 by John von Neumann Institute for Computing
Permission to make digital or hard copies of portions of this work for personal or classroom use is granted provided that the copies are not made or distributed for profit or commercial advantage and that copies bear this notice and the full citation on the first page. To copy otherwise requires prior specific permission by the publisher mentioned above.

http://www.fz-juelich.de/nic-series/volume32

Structural and Electronic Properties of Clean and Adsorbate-Covered (001) Surfaces of Cubic SiC

Xiangyang Peng, Jürgen Wieferink, Peter Krüger, and Johannes Pollmann

Institut für Festkörpertheorie
Wilhelm-Klemm-Str. 10, 48149 Münster, Germany
E-mail: {pengx, wiefer, kruger, pollman}@uni-muenster.de

We report *ab initio* calculations on the atomic and electronic structure of clean and adsorbate-covered SiC(001) surfaces carried out within local density approximation of density functional theory. First we present a general structure model for clean SiC(001)-($n\times2$) surfaces that allows us to identify the origin and nature of the $n\times2$ reconstructions and to rationalize the occurrence of Si addimer nanostrings. Next, we discuss acetylene adsorption on SiC(001)-(2×1). Finally, we consider hydrogen adsorption on SiC(001)-(3×2) which has recently moved into the focus of interest because of the discovery of hydrogen-induced surface metallization.

1 Introduction

Silicon carbide (SiC) is a wide-band gap compound semiconductor with intriguing properties. It has very promising potential for applications in microelectronics and electrooptical devices[1,2]. For example, blue light emitting diodes, high-frequency devices and sensors working in harsh environments are only the first steps in the application of SiC as an advanced material. Consequently, SiC is now in the focus of detailed experimental and theoretical investigations[1–5]. From a fundamental point of view SiC is unique in that it is a fairly ionic group-IV compound semiconductor. In particular, SiC is found to occur in an extremely large number of polytypes. Among these cubic β-SiC appears to be very important for technological use.

The very basis for most of the applications is the growth of high quality crystals which turns out to be a formidable task. For a precise control of processes relevant in SiC growth a detailed understanding of structural and electronic properties of SiC surfaces is highly desirable. Ideal bulk-truncated SiC(001)-(1×1) surfaces are terminated either by a Si or a C layer. At real SiC(001) surfaces more than ten different reconstructions have been observed depending on surface stoichiometry and surface preparation conditions[2,3]. Quite a number of structural models for explaning the observed reconstructions has been suggested on the basis of experimental results[2,3]. Yet, more detailed investigations have shown that a quantitative determination of the atomic structure of clean SiC(001) surfaces remains to be a major challenge[4,5].

Adsorption of organic materials on semiconductor surfaces opens up entirely new fields of applications in microelectronics. The combination of organic chemistry and semiconductor technology has the potential to realize customized devices for special applications[6,7]. In this context SiC is an attrative substrate for the adsorption of organic molecules because of its extraordinary bulk properties, its biocompatibility making it interesting for sensor devices, and its surface reactivity which is completely different from that of Si. By using appropriately reconstructed SiC surfaces as a substrate, organic molecules that can not be bound to a Si surface may be chemisorbed on SiC.

Recently, nanochemistry of SiC surfaces has attracted considerable interest. In particular, hydrogen adsorption has led to very surprising results that are not fully understood at present. Derycke at al.[8] have shown that molecular hydrogen readily adsorbs on SiC(001)-c(4×2) while it hardly interacts with SiC(001)-(3×2) although both surfaces are characterized by similar dimers. In addition, adsorption of atomic hydrogen which usually saturates dangling bonds and eliminates surface states from the band gap making the surface semiconducting leads to an amazing metallization of the SiC(001)-(3×2) surface[9].

Our project is devoted to a thorough *ab initio* study of the structural and electronic properties of clean and adsorbate-covered SiC(001) surfaces in order to determine reliable structural models for the clean surfaces, as well as to contribute to a better understanding of the anticipated functionalization of SiC surfaces by hydrocarbon adsorption and of the observed hydrogen-induced metallization of SiC(001)-(3×2). After a brief outline of our computational method in Sec. 2 we discuss in Sec. 3 some results of our extensive calculations for clean SiC(001) surfaces. From these investigations a generalized model emerges that describes the different observed $n\times2$ reconstructions in a unified way. In Sec. 4 we address acetylene adsorption on SiC(001)-(2×1) and in Sec. 5 we discuss the hydrogen-induced metallization of the SiC(001)-(3×2) surface.

2 Calculational Method

Our calculations are carried out in the framework of density functional theory within local density approximation[10]. The electron-ion interaction is described by norm-conserving pseudopotentials[11] in separable form. The surface systems are represented by supercells containing slabs of 8 to 18 SiC layers and one layer of H atoms saturating the bottom layer of each slab to avoid artificial gap states. The top layers contain appropriate numbers of adatoms. A vacuum region larger than 10 Å is used to decouple neighboring supercells[5,12].

We expand the wave functions in a set of Gaussian orbitals with s, p, d and s^* symmetry. This very efficient basis set leads to a generalized eigenvalue problem with matrices that are about fifty times smaller than those occuring in a plane wave approach. The charge density and the local part of the potential are represented in Fourier space. Therefore, the integrals determining the matrix elements of the Hamiltonian can be evaluated analytically. The short-range nonlocal part of the pseudopotentials is treated in real space. The electrostatic potential of the supercell is calculated using Poisson's equation in a Fourier representation and by a subsequent Fast-Fourier-Transformation to real space using a grid with spacings of 0.16 Å. Structure optimizations are carried out employing Hellmann-Feynman, as well as Pulay forces[5,13]. The relative stability of surfaces with different numbers of atoms is compared by an analysis of the grand-canonical potential within the scheme suggested by Qian, Martin and Chadi[14].

Within our approach the calculation of the charge density, the evaluation of the Hamiltonian matrix elements by summation of all Fourier components and the estimation of the forces are the most time consuming parts of computation. However, these parts of our code are massively parallelized with respect to the points of the grids in real or Fourier space, respectively.

3 Generalized Reconstruction Model of SiC(001)-(n×2) Surfaces

Real Si-terminated SiC(001) surfaces, prepared by annealing SiC in a flux of Si atoms, show many different reconstructions ranging from the stoichiometric 2×1 over 3×2, 5×2, 7×2, ... up to 15×2 surfaces[2,3]. For quite some time it was believed, therefore, that SiC(001) shows only n×2 reconstructions with odd n. More recently, however, Douillard *et al.*[15] observed an 8×2 reconstruction and even more interestingly the formation of Si nanostrings on SiC(001) surfaces raising the questions whether n×2 reconstructions with even n are possible, in general, and why Si nanostrings can occur at all. Therefore, one aim of our project is to elucidate the atomic configurations in the observed n×2 superstructures and to explain their amazing order with respect to Si adatom coverage. Likewise, we want to rationalize the occurrence of Si nanostrings and identify their physical nature.

We have studied the reconstructions of the c(4×2), 3×2 and 5×2 surfaces by *ab initio* calculations, previously, and have suggested structural models following from minimum surface formation energy in each case[12,16,17]. These models are in good agreement with a host of experimental data. Employing these results we have been able to derive a general n×2 reconstruction model which is based on two structural building blocks only, which we label A and B. They are characteristic for the c(4×2) surface (A) and the 3×2 surface (B), respectively. Our optimized c(4×2) missing row asymmetric dimer model[16] has half a monolayer (ML) of Si adatoms adsorbed on the complete Si sublayer forming rows of buckeled Si adimers in the ×2 direction. Each second addimer row is missing. In our 3×2 two adlayer asymmetric dimer (TAAD) model[12] two partial layers of Si adatoms are adsorbed on the clean surface. Two Si adatoms per unit cell in the top adlayer form one buckled dimer in the 3× direction while four Si atoms in the second adlayer form two weak Si dimers in the ×2 direction. For the 5×2 reconstruction we also find a TAADM as the optimal structure[17]. Comparing the three optimized reconstructions, it occured to us that the building block of the 5×2 reconstruction is a mere superposition of the building blocks A and B of the other two reconstructions. The atomic positions in the 5×2 unit cell turn out to be virtually the same as those in the respective A and B building blocks of the c(4×2) and (3×2) surfaces. On the basis of these *ab initio* results we were led to the expectation that all higher n×2 reconstructions are just appropriate superpositions of A and B building blocks.

Therefore, we have extrapolated our TAADM to higher n values and suggest that n×2 reconstructions are simply appropriate superpositions of A- and B-type building blocks. In the general n×2 model with $n > 3$ each reconstruction contains l A-type and m B-type building blocks whereby $n = 2 \cdot l + 3 \cdot m$ with $l \geq 1$ and $m \geq 1$. To corroborate this idea we have carried out very demanding *ab initio* calculations on 7×2 and 8×2 reconstructions investigating a host of conceivable surface structures. In the latter case there are 158 atoms per supercell leading, e. g., to 3300×3300 Hamiltonian matrices. For both surfaces we find our TAADM to be the locally stable energy-minimum configuration. The optimized structures are shown in Fig 1 (a). Both reconstructions consist indeed of A- and B-type building blocks with atomic positions very similar to those in the respective c(4×2) and 3×2 reconstructions. The optimized 7×2 and 8×2 structures are obviously AAB and ABB reconstructions, respectively. The 8×2 structure exhibits one D_A and two D_B addimers per surface unit cell. The D_B dimers reside significantly higher above the surface than the D_A dimers (see the side view in Fig. 1 (a)) giving rise to pairs of Si addimer nanolines in an

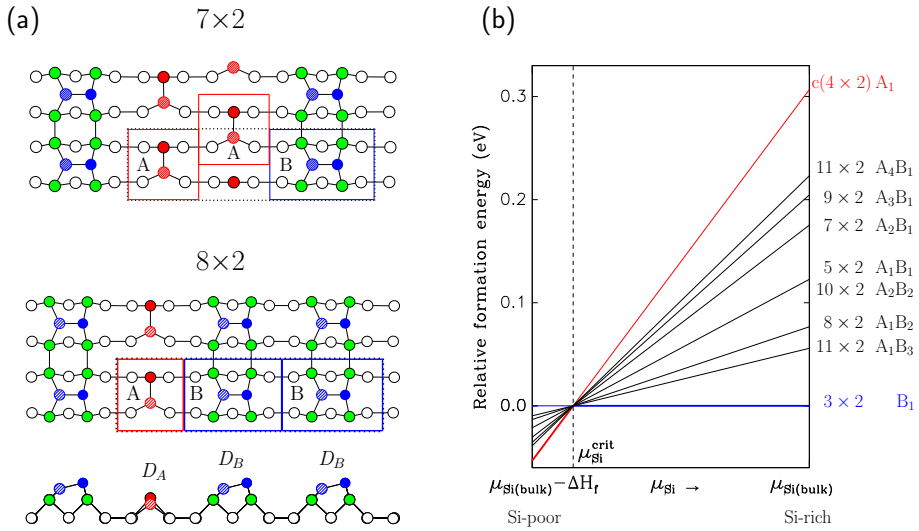


Figure 1. (a) Top views of the optimal surface structure of the 7×2 and 8×2 TAAD models of SiC(001). For the 8×2 TAADM a side view is shown, as well. The atoms of the Si sublayer are shown by open circles. Building blocks A and B are indicated by red squares and blue rectangles, respectively. (b) Relative formation energies per 1×1 unit cell of the c(4×2) and n×2 surfaces (referred to the 3×2 reconstruction) as a function of μ_{Si}.

8×2 periodic arrangement in very nice agreement with STM experiments[15].

The formation energies of some n×2 reconstructions with n up to 11 are shown in Fig. 1 (b) as functions of the chemical potential μ_{Si} of Si in the gas phase. The decompositions of these structures in A and B blocks is given in the figure, as well. Note that, e. g., the 11×2 surface has two realizations differing in adatom coverage. For Si-poor and Si-rich conditions the c(4×2) and 3×2 reconstructions are lowest in formation energy, respectively. All other n×2 reconstructions fall in between these two limits. Our general TAADM explains a wealth of observations on n×2 surfaces as discussed in detail elsewhere[18]. In particular, it shows in agreement with experiment that neither a primitive 4×2 nor a 6×2 reconstruction occurs. Other n×2 reconstructions with larger even n are possible, however. Moreover, it allows us to rationalize the occurrence of a wealth of periodic and nonperiodic Si addimer nanostrings, as observed in experiment[15].

4 Adsorption of Acetylene on SiC(001)-(2×1)

The SiC(001) surface offers a broad range of adsorption channels for organic molecules due to its rich variety of reconstructions. In this brief report we focus on acetylene (C_2H_2) adsorption on SiC(001)-(2×1). In particular, we show that acetylene experiences a completely different bonding configuration on SiC(001)-(2×1) than on the Si(001)-(2×1) surface. Fig. 2 (a) gives an overview of the investigated sites for acetylene adsorption. Acetylene has a C≡C triple bond consisting of one σ and two π bonds. The two π bonds are

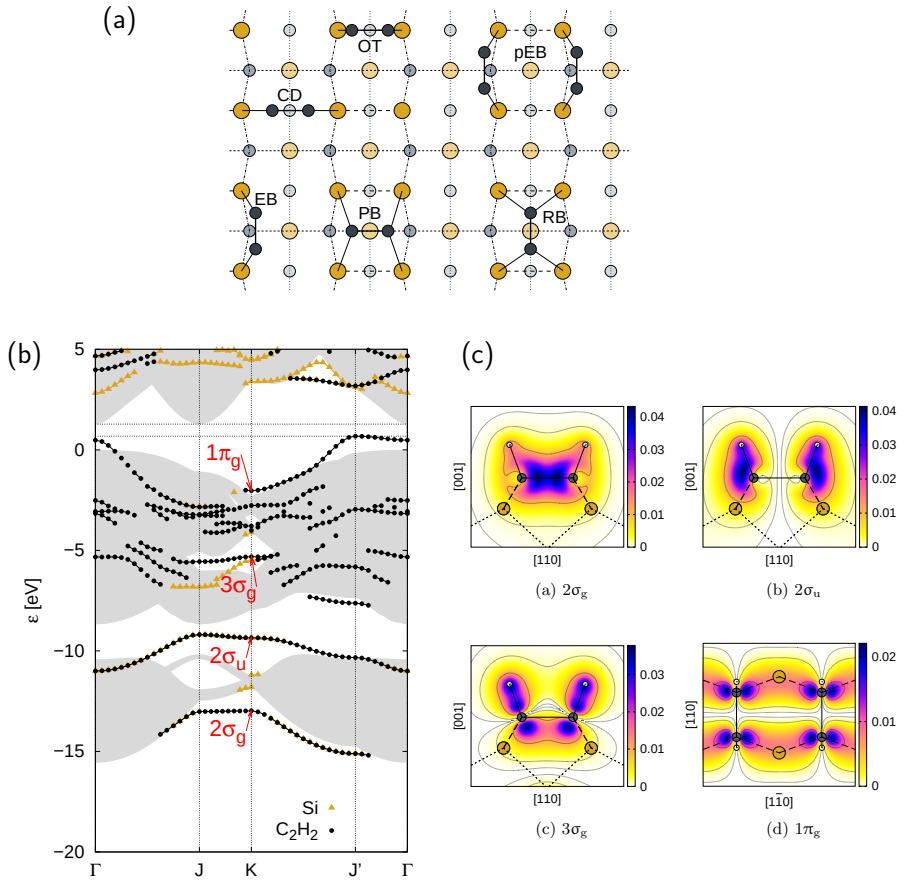


Figure 2. (a) Top view of the Si-terminated SiC(001)-(2×1) surface with various adsorption sites for acetylene. Hydrogen atoms are omitted for clarity. Carbon atoms of adsorbed molecules are shown by black dots. Large ocher and light ocher circles depict Si atoms on the first and third substrate layers while small blue and light blue circles indicate C atoms on the second and fourth substrate layers, respectively. (b) Surface band structure of an acetylene monolayer on SiC(001) in the (1×2)-RB configuration. States that are strongly localized at the adsorbed C_2H_2 molecules are indicated by black dots. (c) Charge-density distributions of the $2\sigma_g, 2\sigma_u, 3\sigma_g$, and $1\pi_g$ states at the K-point.

highly reactive and interact preferentially with surface dangling bonds, therefore. In the so called di-σ configurations acetylene is bonded to two Si atoms at the surface and a C=C double bond is retained in the molecule. These di-σ configurations lead to *cross dimer* (CD), *on top* (OT), *end bridge* (EB) and *paired end bridge* (pEB) structures. Alternatively, acetylene can be adsorbed at the surface by formation of four σ bonds between each molecule and the four Si atoms of two neighboring Si dimers leading to tetra-σ configurations. These are called *pedestal bridge* (PB) and *rotated bridge* (RB) structures.

Our investigations[19] show that acetylene adsorbs preferentially in rotated-bridge sites on SiC(001). In the optimal (1×2)-RB surface structure (not shown for shortness) each surface Si atom is bound to two C atoms of two neighboring acetylene molecules and two

C atoms on the second substrate layer. This way all atoms of the molecule and the substrate become fully coordinated. The band structure for the optimized configuration is shown in Fig. 2 (b). There are four bands of localized surface states which we label according to the corresponding orbitals of the free molecule. The bonding and antibonding states formed by the carbon σ-orbitals give rise to the bands $2\sigma_g$ and $2\sigma_u$ which show a strong dispersion along the ΓJ and KJ' direction due to the interaction between carbon σ-orbitals of neighboring molecules at the surface. Respective charge densities at the K-point are shown in the upper panels of Fig. 2 (c). The flat band $3\sigma_g$ near -5 eV mostly stems from the C-H bonds of the adsorbed acetylene molecules (see lower left panel of Fig. 2 (c)). In addition, the adsorption of acetylene leads to a hybridization of the lowest unoccupied π-orbitals of the molecule with the former Si dangling bonds of the surface. Band $1\pi_g$ results from one linear combination of these bonding orbitals (see lower right panel of Fig. 2 (c)). While acetylene perfectly fits into the center between four Si atoms at the SiC(001)-(2×1) surface, on Si(001) it adsorbes preferentially in (2×2)-pEB and (2×1)-OT configurations. Due to the correspondingly larger lattice constant of Si a strong bending of the Si-C bonds would be necessary to achieve a RB structure at the latter surface.

5 Hydrogen-Induced Metallization of the SiC(001)-(3×2) Surface

Turning a semiconducting surface into a metallic one by H adsorption is generally deemed very unlikely. Yet, recent experiments have provided clear evidence for the metallization of SiC(001)-(3×2) by hydrogenation[9]. To explain these findings, Derycke *et al.*[9] conjectured that the top adlayer Si dimers in the TAADM become saturated, at first, by formation of monohydrides. Further H adatoms were assumed to break the Si dimers in the third layer and to become bonded to one of the two Si atoms of the broken dimers, leaving a Si dangling bond at the other. Within this scenario the Si dangling bonds on the third layer are stabilized by steric hindrance and would lead to surface metallization. Very recently, this explanation has been questioned on the basis of several *ab initio* studies[20–23] which find that the lattice configuration suggested by Derycke *et al.* for the metallic surface is not stable. The calculations show that H adsorbs in the optimized structure at the topmost Si layer forming monohydrides and additional H atoms adsorb on the third layer forming angular Si-H-Si bonds. These bonds are only partially saturated leading to a surface band structure which is clearly metallic. We have found that this structure is not the only one leading to a metallic surface. In a systematic DFT study[23] we have scrutinized a number of conceivable geometries for several degrees of H exposure. We find that H atoms can also occupy bridge positions in angular Si-H-Si bonds on the second layer inducing metallization, as well. Our results show in addition that the formation of Si dihydrides instead of monohydrides at the surface leads to an even more favorable grand canonical potential at high H exposures.

As an example, Fig 3. (a) shows a top and a side view of the optimized structure for large H exposure. The Si-H bond lengths and the angles between the two Si-H bonds on the second (third) layer are 1.67 Å (1.66 Å) and 151° (127°), respectively. The corresponding surface band structure is shown in Fig. 3 (b). It clearly reveals that this adsorption configuration has a metallic surface. The adsorption of H on the second and third layer leads to the bands B_1, B_2 and B_3. The former two of these bands are located within the gap showing a large dispersion. Around the M and J' points the states B_1 and B_2 are mainly localized on the second layer. The band B_3 stems from Si-H-Si bonds on the third layer. Fig. 3 (c)

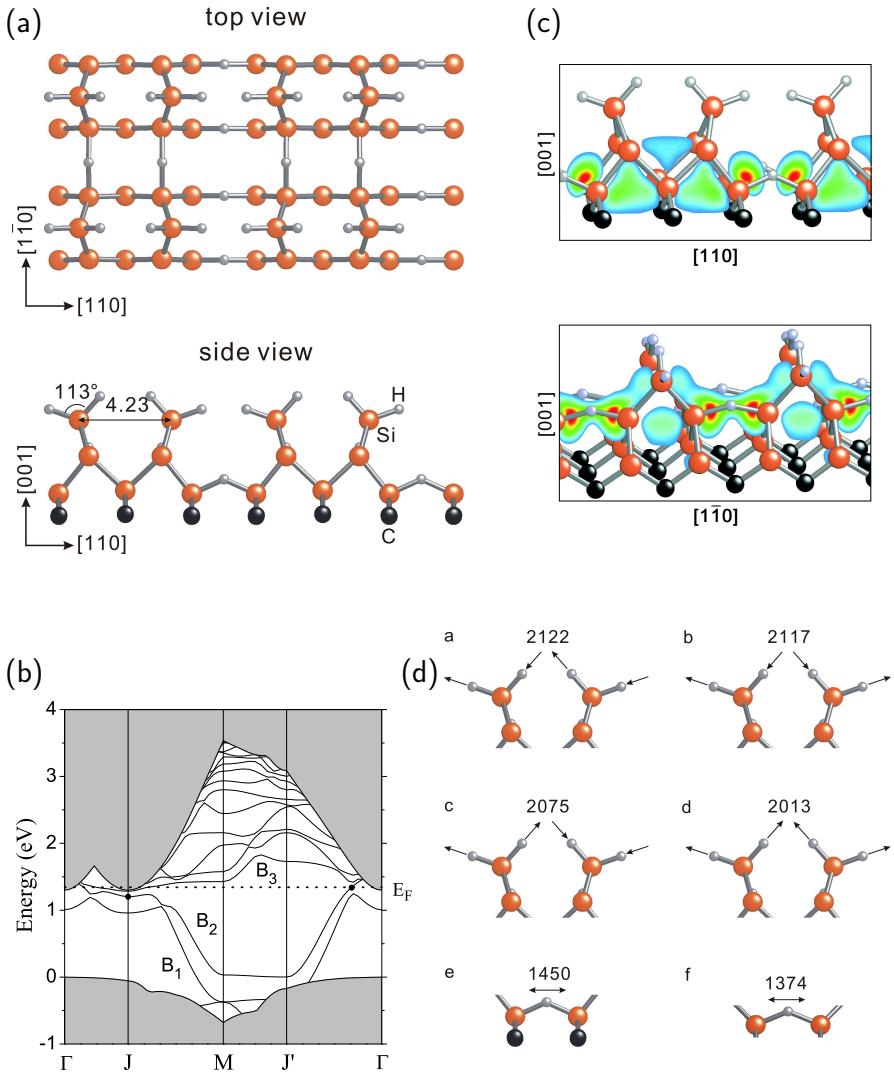


Figure 3. (a) Top and side view of the optimized H-induced metallic structure. The top dimers are broken and two canted dihydride units are formed per unit cell due to H adsorption at the top layer. The second and third layer dimers are also broken establishing angular Si-H-Si bonds with H atoms in bridge positions. (b) Corresponding surface band structure along high-symmetry lines of the surface Brillouin zone. The dots indicate states whose charge-density distributions are shown in (c). Displacement patterns of a few salient hydrogen-related vibrational modes are depicted in (d).

shows the charge density of B_2 states near the Fermi level at the J point and close to the Γ point. At J the state is strongly localized on the third layer Si-H-Si bonds (see top panel) while near Γ it is mainly localized on the second layer Si-H-Si bonds (see bottom panel). Thus the wave function character of the states in the B_2 band changes entirely from J to

the region near Γ. Band B_1 is fully occupied. The bands B_2 and B_3 are only partially occupied and cross the Fermi level giving rise to the metallic surface.

We have also calculated surface phonons at the Γ point. Fig. 3 (d) shows the displacement patterns of salient hydrogen-related vibrational modes. The four modes above 2000 cm^{-1} are antisymmetric or symmetric vibrations within or between the dihydride units. These phonon energies are close to typical energies of Si-H stretch vibrations. In contrast, the frequencies of the highest vibrational modes related to H atoms in the angular Si-H-Si bonds on the second (1374 cm^{-1}) and third layer (1450 cm^{-1}) are comparatively low. This is related to the fact that the Si-H bonds in the bridge bonds are much longer (1.67 Å) and thus much weaker than a usual short (1.50 Å) and strong Si-H bond. These fingerprints of the Si-H-Si bonds in the calculated phonon spectrum have not been observed to date[24], possibly due to a restricted experimental resolution in the low frequency range.

Acknowledgments

Grants of computer time from the John von Neumann Institute, Jülich, and financial support of this work by the Deutsche Forschungsgemeinschaft are gratefully acknowledged.

References

1. W. J. Choyke, H. Matsunami, and G. Pensl (eds.) *Silicon Carbide, Fundamental Questions and Applications to Current Device Technology* Springer, Berlin (2004).
2. P. G. Soukiassian and H.B. Enriquez, J. Phys.: Condens. Matter **16**, S1611 (2004).
3. V. Bermudez, phys. stat. sol. (b) **202**, 447 (1997).
4. A. Catellani and G. Galli, Prog. Surf. Sci. **69**, 101 (2002).
5. J. Pollmann and P. Krüger, J. Phys.: Condens. Matter **16**, S1659 (2004).
6. S.F. Bent, Surf. Sci. **500**, 879 (2002).
7. J. Yates, Science **279**, 335 (1998).
8. V. Derycke *et al.*, Phys. Rev. B **63**, R201305 (2001).
9. V. Derycke *et al.*, Nature Mat. **2**, 253 (2003).
10. W. Kohn and L.J. Sham, Phys. Rev. **140**, A1133 (1965).
11. D.R. Hamann, M. Schlüter, and C. Chiang, Phys. Rev. Lett. **43**, 1494 (1979).
12. W. Lu, P. Krüger, and J. Pollmann, Phys. Rev. B **60**, 2495 (1999).
13. P. Krüger and J. Pollmann, Phys. Rev. B **38**, 10578 (1988).
14. G.X. Qian, R. M. Martin, and D.J. Chadi, Phys. Rev. B **38**, 7649 (1988).
15. L. Douillard *et al.*, Surf. Sci. **401**, L395 (1998).
16. W. Lu, P. Krüger, and J. Pollmann, Phys. Rev. Lett. **80**, 2090 (1998).
17. W. Lu, P. Krüger, and J. Pollmann, Phys. Rev. B **61**, 2680 (2000).
18. P. Krüger and J. Pollmann, Phys. Rev. B (in print).
19. J. Wieferink, P. Krüger, and J. Pollmann, submitted to Phys. Rev. B.
20. R. Di Felice *et al.*, Phys. Rev. Lett. **94**, 116103 (2005).
21. F.B. Mota *et al.*, J. Phys.: Condens. Matter **17**, 4739 (2005).
22. H. Chang, J. Wu, B.-L. Gu, F. Liu, and W. Duan, Phys. Rev. Lett. **95**, 196803 (2005).
23. X. Peng, P. Krüger, and J. Pollmann, Phys. Rev. B (in print).
24. F. Amy and Y.J. Chabal, J. Chem. Phys. **119**, 6201 (2003).